ASTM INTERNATIONAL



Materials Performance and Characterization

Marcos Ariel Mata-Rodríguez,[1] Marco Arturo García-Rentería,[1] Ricardo Rafael Ambríz-Rojas,[2] José Ángel Cabral-Miramontes,[3] Victor Hugo López-Morelos,[4] Maria del Carmen Ramírez-López,[4] and Francisco Fernando Curiel-López[5]

**DOI: 10.1520/MPC20220035**

# Microstructural Evolution of Inconel 718 during Aging and Its Correlation with Electric Conductivity Measurements

VOL. 11 / NO. 1 / 2022

Materials Performance and Characterization

doi:10.1520/MPC20220035 / Vol. 11 / No. 1 / 2022 / available online at www.astm.org



Marcos Ariel Mata-Rodríguez,[1] Marco Arturo García-Rentería,[1] Ricardo Rafael Ambríz-Rojas,[2] José Ángel Cabral-Miramontes,[3] Victor Hugo López-Morelos,[4] Maria del Carmen Ramírez-López,[4] and Francisco Fernando Curiel-López[5]

# Microstructural Evolution of Inconel 718 during Aging and Its Correlation with Electric Conductivity Measurements

Manuscript received March 30, 2022; accepted for publication July 13, 2022; published online September 23, 2022. Issue published September 23, 2022.

[1] Universidad Autónoma de Coahuila, Carr. 57, Km 5, C.P. 25720, Monclova, Coahuila, México

[2] Instituto Politécnico Nacional CIITEC-IPN, Cerrada de Cecati S/N Col. Sta. C.P. 02250 Catarina, Azcapotzalco, Ciudad de México, México

[3] Universidad Autónoma de Nuevo León, Av. Universidad S/N. Ciudad Universitaria. C.P. 66455 San Nicolás de los Garza, Nuevo León, México

[4] Instituto de Investigación en Metalurgia y Materiales, Universidad Michoacana de San Nicolás de Hidalgo, A.P. 888, CP 58000, Morelia, Michoacán, México

[5] Instituto de Investigación en Metalurgia y Materiales, Universidad Michoacana de San Nicolás de Hidalgo, A.P. 888, CP 58000, Morelia, Michoacán, México (Corresponding author), e-mail: francisco.curiel@umich.mx, https://orcid.org/0000-0002-7849-8051

## Reference

M. A. Mata-Rodríguez, M. A. García-Rentería, R. R. Ambríz-Rojas, J. A. Cabral-Miramontes, V. H. López-Morelos, M. C. Ramírez-López, and F. F. Curiel-López, "Microstructural Evolution of Inconel 718 during Aging and Its Correlation with Electric Conductivity Measurements," *Materials Performance and Characterization* 11, no. 1 (2022): 267–277. https://doi.org/10.1520/MPC20220035

## ABSTRACT

The microstructural evolution of the nickel-base superalloy Inconel 718 after exposition at 750°C for different holding times (10 min–1,000 h) was characterized and correlated with the Eddy current (EC) technique. The results showed that electrical conductivity increases with aging time. This behavior was associated with the precipitation and coarsening of the metastable γ″ phase and its transformation into the detrimental δ phase after 100 h. EC nondestructive evaluation was correlated with X-ray diffraction patterns in terms of the precipitation and growth of secondary carbides that were observed in the scanning electron microscope. Vickers microhardness values were also in agreement with microstructural changes and EC measurements, as the maximum hardened condition can be associated with the precipitation of secondary phases before the transformation of the γ″ phase into the δ phase.

## Keywords

microstructure, X-ray diffraction, hardness, scanning electron microscopy, Inconel

# Introduction

Nickel-based superalloys are very attractive engineering materials used in a wide range of applications because of their corrosion resistance and mechanical properties at high temperatures.[1,2] The principal intermetallic phases in the Inconel 718 nickel-base alloy that provide high mechanical performance are the gamma prime ($\gamma'$, cubic structure, $Ni_3Al$), gamma bi-prime ($\gamma''$, orthorhombic structure) and MC type carbides (NbC and TiC).[3–5] The mechanical properties of this alloy at high temperatures are improved by precipitation-strengthening due to the reaction $\gamma \rightarrow \gamma' + \gamma''$.[6] However, the transformation of the metastable $\gamma''$ phase into the $\delta$ phase tends to promote failure of components because of the decrement in tensile strength and ductility.[7,8]

The use of nondestructive evaluation (NDE) methods, such as the ultrasonic test, Eddy current (EC), and thermoelectricity (TE), have been used to detect microstructural changes on superalloys. These techniques allow for the detection of microstructural changes that can be used to assess the state of structural components after thermal exposure.[9–13] The EC technique is a highly sensitive method based on conductivity changes that are dependent on the microstructural characteristics of the materials. EC involves impedance variation measurements of a transducer that induces magnetism or voltage. Thus, the changes in conductivity may be associated with the different microstructural characteristics of the materials.[14] The International Annealed Copper Standard (IACS) establishes that conductivity can be expressed in percent of IACS (%IACS), which can be measured from any metallic material relative to pure copper.[15] The changes in this property because of microstructural evolution resulting from the precipitation and growth of secondary phases can be detected by using EC. For instance, the use of swept frequencies can determine the surface stress condition on Inconel 718 shot peened under different heat treatments.[16] Pereira et al.[17] used a transmit-receive configuration test to determine the microstructural changes in Inconel 718 exposed to different temperatures where the presence of $\gamma'$, $\gamma''$ and $\delta$ phases, as well as MC carbides, induced quantitative changes in the conductivity of the material. Those changes were associated with the scattering of electrons produced by intermetallic phases in short times of aging. Changes in the lattice parameter over short distances due to distortion of the crystal lattice by diffusion processes can alter the conductivity of nickel-base alloys.[18] Additionally, EC has been used to determine the microstructural characteristics for other materials. For instance, Silva et al.[19] detected the amount of magnetic martensite phase on cold-worked AISI 321 stainless steel. Camerini et al.[20] studied the sigma and delta phases in thermally aged superduplex stainless steel. Still, the application of EC as a sensitive technique to detect microstructural evolution in Inconel 718 (aged at 750°C for 0.16–1,000 h) has not been evaluated. In this context, the objective of this research is to propose the application of the EC technique to correlate the evolution of the $\gamma''$ phase using conductivity measurements (%IACS), XRD patterns, microscopy, and microhardness measurements.

# Materials and Methods

### HEAT TREATMENT

Hot-rolled and annealed Inconel 718 plates ($10 \times 10 \times 4$ mm$^3$) at 950°C were used. The chemical composition of the material was determined by optical emission spectroscopy, which corresponds to 0.05 C, 18.95 Cr, 54.0 Ni, 3.13 Mo, 0.040 Cu, 0.70 Al, 0.084 Mn, 0.091 Si, 1.10 Ti, 5.1 Nb, and 16.75 Fe (wt. %). Samples were heat-treated by solution at 1,050°C for 1 h and then quenched in water at 25 ± 1°C to dissolve the $\delta$ phase.[21] Subsequently, the samples were tightly enveloped with stainless steel and placed in a muffle furnace at room temperature. The samples were heated at 5°C/min to 750°C, held at temperature during different times (0.16, 1, 10, 100, 250, 500, and 1,000 h), and finally cooled in air to room temperature, as illustrated in figure 1.

### MICROSTRUCTURAL CHARACTERIZATION

Microstructural characteristics of the Inconel 718 base metal (BM) and the aged samples were obtained by using optical microscopy (OM), scanning electron microscopy (SEM), and XRD. To determine the microstructural

**FIG. 1**

Heat treatment cycle of the Inconel 718 samples.

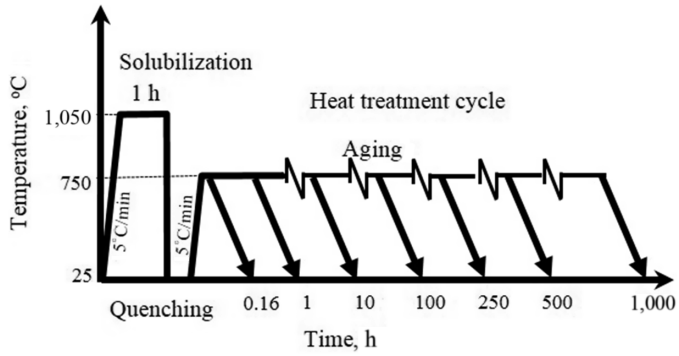


characteristics, the specimens were prepared using plain metallographic techniques (machining the surface, mechanical grinding with emery paper and polishing with diamond paste to obtain a mirror-like surface). To reveal the microstructure, the samples were chemically etched by immersion (1 to 3 min) in a solution of $HNO_3$ + HCl + $H_2SO_4$[22] and then rinsed with deionized water, ethanol, and air dried. Before the SEM observations, the samples were washed in an ultrasonic bath with the same cleaning procedure.

To identify the precipitation sequence of the secondary phases due to the heat treatment, XRD patterns were obtained in a diffractometer employing $Cu_\alpha$ radiation. The acquisition conditions were: 2θ angle range = 30° to 100°, anlge steps = 0.01°, step time = 6 s.

### VICKERS MICROHARDNESS MEASUREMENTS

Vickers microhardness (HV) measurements were performed with a load of 500 g applied during 15 s. A total of ten indentations were performed at the center for each sample. The arithmetic mean value was plotted for each condition as a function of aging time to correlate with the microstructural evolution.

### EC MEASUREMENTS

The conductivity (in %IACS) was measured with an OmniScan MX NDE equipment with a variable voltage source. Previously, the equipment was calibrated for different materials used as standards. **Figure 2*A*** shows the imaginary component (reactance) for the voltage induced as a function of the real component ratio (resistivity). **Figure 2*B*** shows the conductivities for different materials, representing the changes associated with the electrical resistivity and the magnetic permeability of the materials and their conditions.[14] The measurements were acquired by a probe 6.35 mm in diameter using a frequency of 500 MHz. The probe was located directly on the surface at the center of the samples. Before performing the measurements, the samples were prepared by mechanical grinding and polished to obtain a surface roughness of ±1 μm. The samples were cleaned and degreased before data reading. Fifty readings were obtained for each specimen; the average was reported as a function of aging time.

## Results and Discussion

### MICROSTRUCTURAL CHARACTERIZATION

**Figure 3** shows the microstructure of the BM and the samples aged at 750°C. The microstructure shows a typical grain structure constituted by equiaxed grains, twin grains (due to the thermomechanical process), and intermetallic precipitates (dark dots). For the BM microphotograph (**fig. 3*A***), the grain size was ~50 μm with a standard deviation of 18 μm; also, the presence of some precipitates homogeneously dispersed (showed as dark particles) was observed. After solutioning (1 h at 1,050°C) and aging the samples at 750°C during 0.16 h

**FIG. 2**

(*A*) EC equipment calibration for different materials and (*B*) conductivity in %IACS of different materials.

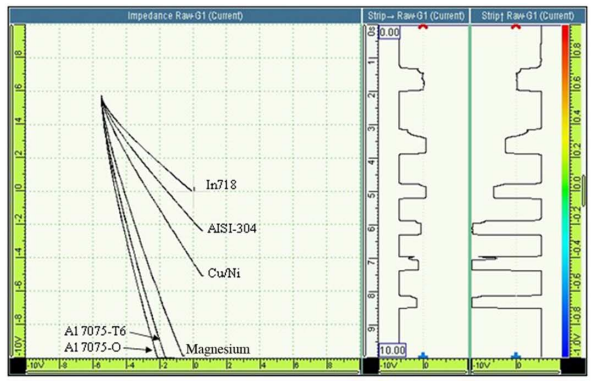


(*A*)

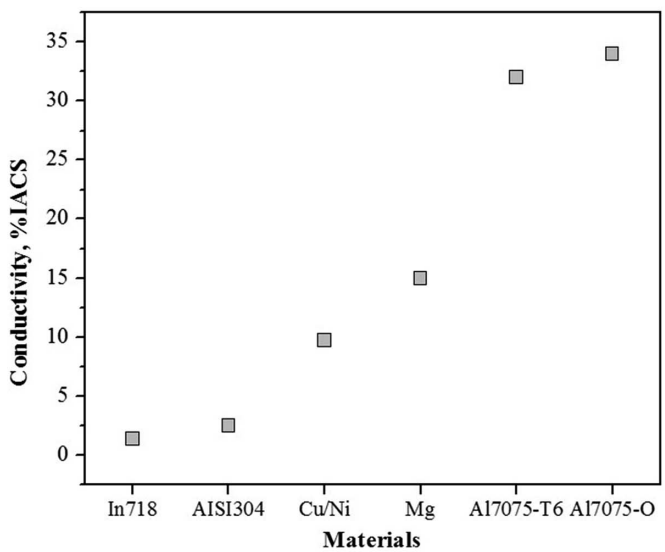


(*B*)

(fig. 3*B*), the grain size tended to grow up to ~110 μm because of the solution heat treatment. This phenomenon was attributed to the coalescence of grain boundaries controlled by a diffusion process; i.e., the average grain size increases due to competitive coarsening. The driving force for this process is the minimization of interfacial energy.[23] For the samples exposed at 750°C for aging times of 1, 10, 100, 250, and 500 h (figures 3*C*–*G*), the alloy exhibited good microstructural stability with a grain size between 110 to 120 μm. This phenomenon may be associated with the energy stored in the material of a few grains, where growth is selectively controlled by the presence of delta phase particles hosted at grain boundaries.[24] Nonetheless, after 1,000 h (fig. 3*H*), the grain size increased up to values of close to 170 μm, because of the reduction in the surface area between the δ-γ interface, as well as the reduction in the δ-γ lattice misfit.[25–27]

Figure 4 shows the cumulative frequency plots in percentage distribution measured from OM images for the BM, and the effect of different holding times in the precipitates growth. The area size in $\mu m^2$ of the carbides (dark spots) for different intervals is presented in the abscissa axis, and the cumulative frequency is presented in percent in the ordered axis. It can be observed that in BM, 90 % of the cumulative carbides area corresponds to an interval between 250–300 $\mu m^2$. After solubilization heat treatment at 1050°C, water quenching and aging at

**FIG. 3**

Microstructure of Inconel 718 and samples aged at 750°C for different times: (*A*) BM; (*B*) 0.16 h; (*C*) 1 h; (*D*) 10 h; (*E*) 100 h; (*F*) 250 h; (*G*) 500 h; and (*H*) 1,000 h.

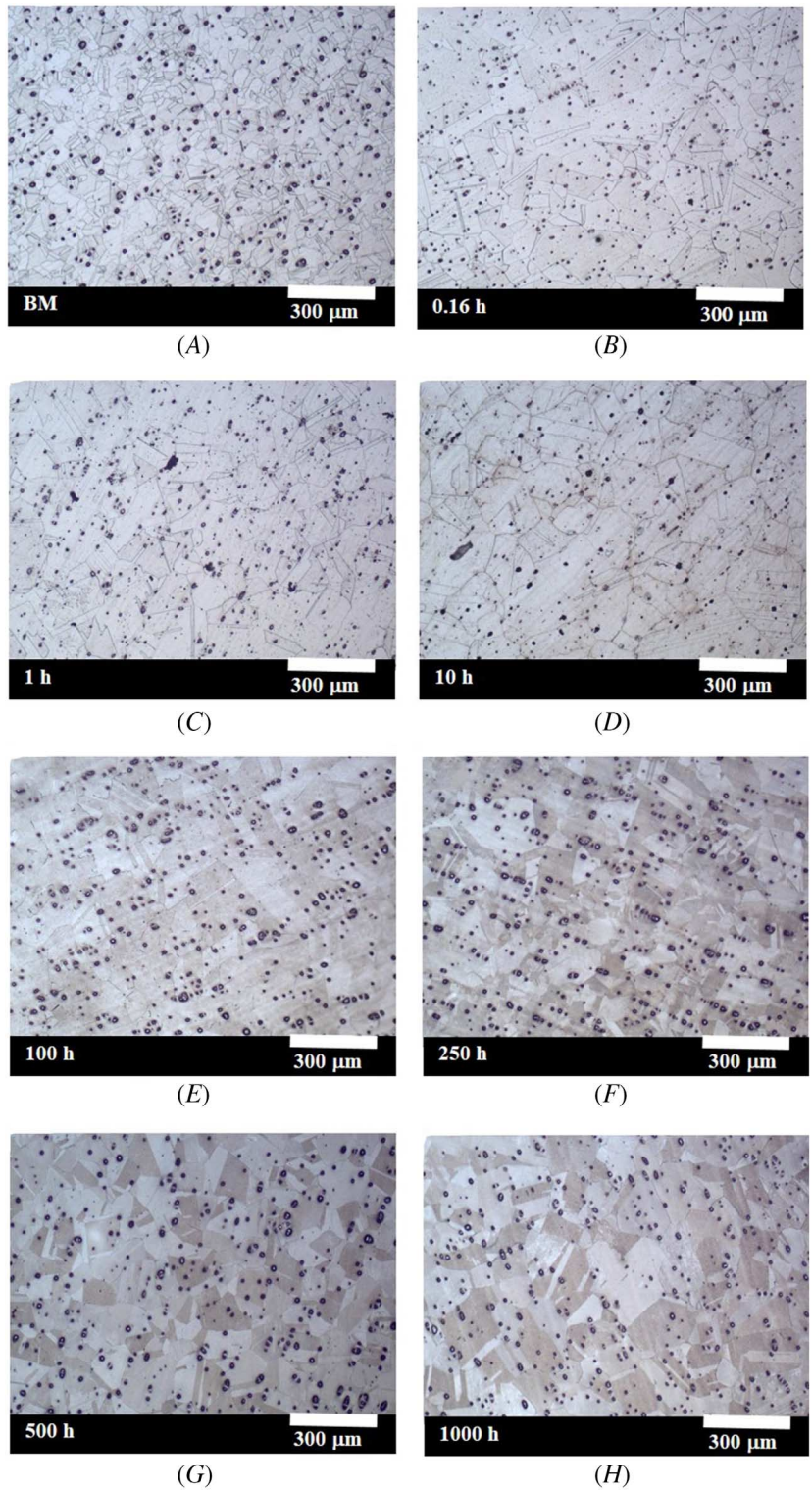

**FIG. 4**

Cumulative frequency versus particle area as a function of heat treatment.

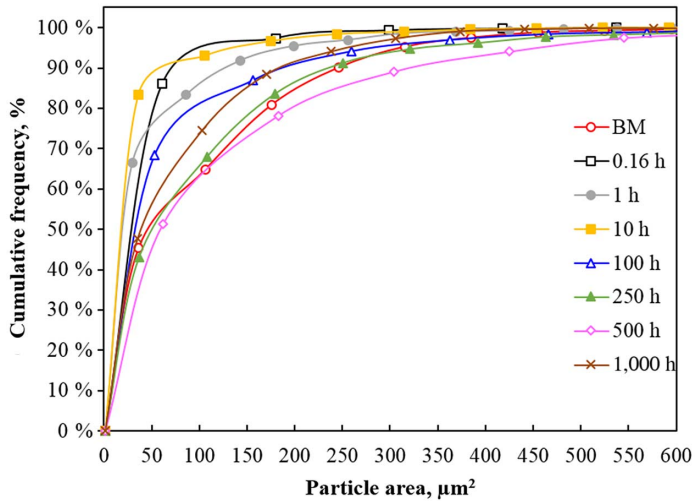


750°C during 0.16, 1, and 10 h, the gradient of the area distribution of the particles was similar, which was reduced to an interval between ~5 to 100 $\mu m^2$, respectively. Whereas, after 250 h, the size of the carbides' area increases up to 200 $\mu m^2$, showing a similar behavior on the slope after 500 h that resembles the condition of the BM. After 1,000 h, a reduction in area between ~150 to 170 $\mu m^2$ was observed. This may be associated with the solute redistribution at the grain boundaries between the matrix and carbides due to long exposure periods at 750°C.

To identify the microstructural characteristics of the matrix and precipitates in terms of distribution and/or evolution of the Inconel 718 BM and the heat-treated samples, SEM was used. **Figure 5** illustrates the photomicrographs obtained at 1,000×. As can be seen, the BM (**fig. 5*A***) exhibits a presence of spheroidal particles (of approximately 15 μm in length) and small precipitates rich in Nb and Ti. An energy dispersive x-ray spectroscopy (EDS) analysis of these particles provided information that closely matches with the stoichiometry of NbC and (Nb,Ti)C.

After solution and aging heat treatment for 0.16 h (**fig. 5*B***), there was no evidence of growth or evolution of primary precipitates, but small grains and stacking faults were consumed by bigger grains. This mechanism is associated with the grain boundaries migration promoting the grain growth, which is also associated with the solution heat treatment.[28] Conversely, it is possible to observe the presence of γ′ phase in the γ-NbC interface in the sample aged at 750°C for 1 h (**fig. 5*C***). This can be linked to the γ′ phase nucleation and growth because these precipitates are formed by elements such as titanium, niobium, and tantalum, which can be substituted by aluminum. This phase is stable only in a narrow range of aluminum/titanium ratios, but titanium and/or niobium can be substituted for up to 60 % of the aluminum.[29] Afterward, at 100 h of exposure, (**fig. 5*D***), intergranular carbides identified as $(Fe,Cr)_{23}C_6$ were found. These secondary carbides act as hardening reinforcement when their distribution is homogenous inside the grains or along twin boundaries, whereas in some cases, they can result in detrimental effects to mechanical properties such as strength, toughness, and ductility.[30] After 500 h, (**fig. 4*E***), the $(Fe, Cr)_{23}C_6$ carbides, in addition to the δ phase, were observed at the grain boundaries. Nonetheless, the δ phase seems to keep growing at 750°C, and once this phase precipitates, it forms Widmanstätten structures, as can be observed in the SEM photomicrographs after a holding time of 1,000 h (**fig. 5*F***).

From the SEM photomicrographs shown in **figure 4**, the Inconel 718 alloy is hardened initially because of the interaction between dislocations and the γ′-phase with an face centered cubic structure ($Ni_3$-Al, Ti or Nb), which is semi-coherent with the matrix. Subsequently, the γ′ phase takes a spherical-like shape with a body centered tetragonal structure ($Ni_3Nb$).[31]

**FIG. 5** SEM of the samples aged at 750°C of Inconel 718: (*A*) BM; (*B*) 0.16 h; (*C*) 1 h; (*D*) 100 h; (*E*) 500 h; and (*F*) 1,000 h.

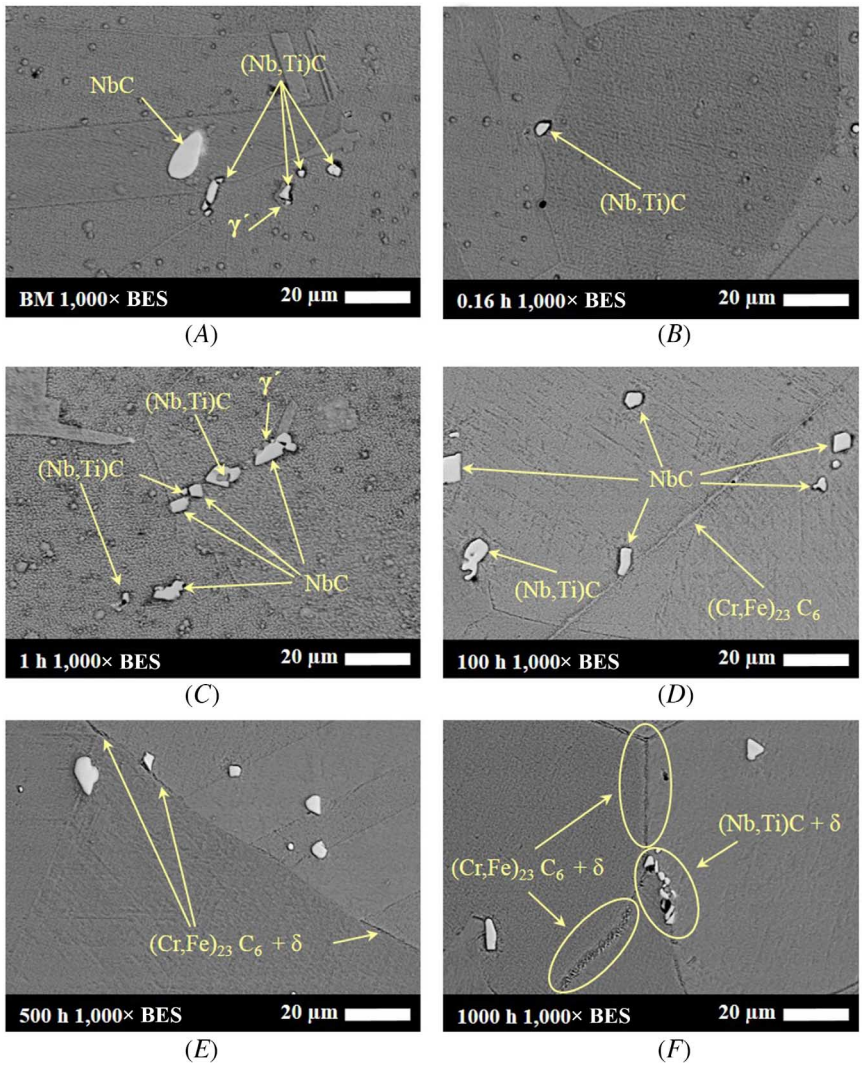


Figure 6*A* shows XRD patterns for the BM and samples aged at 750°C. Figure 6*A* exhibits the typical highest reflection peaks corresponding to the matrix of Inconel 718, whereas shorter reflection peaks correspond to the (Nb,Ti)C particles.[32]

Figure 6*B* shows the XRD patterns at different aging times. The evolution of the MC carbides and γ matrix seems to obey the peritectoid reaction MC + γ → γ′ until 1 h. Afterward, the samples aged for more than 100 h show that carbides of the type $(Fe,Cr)_{23}C_6$ are present in the XRD pattern because of the reaction MC + γ/γ′ → $(Fe,Cr)_{23}C_6$, as a consequence of the deterioration of the MC carbides.[33,34] On the other hand, γ″ ($Ni_3Nb$) nucleates grow at early stages until 1 h of aging, and the δ phase ($Ni_3Nb$) starts to appear after holding at temperature for 10 h because of the transformation of the metastable γ″ ($Ni_3Nb$) tetragonal structure into the orthorhombic δ phase, with the same chemical stoichiometry, which is thermodynamically more stable than γ3″ phase.[35] The evolution of these precipitates correlates with the observation in the SEM, where a thin plate-like of γ′ placed at the MC/γ boundary begins at early stages, followed by the nucleation and growth of $(Fe,Cr)_{23}C_6$ particles at the γ/γ and γ/γ″ interface.

**FIG. 6**

XRD patterns of the Inconel 718 alloy for different conditions: (*A*) base material and (*B*) heat-treated samples.

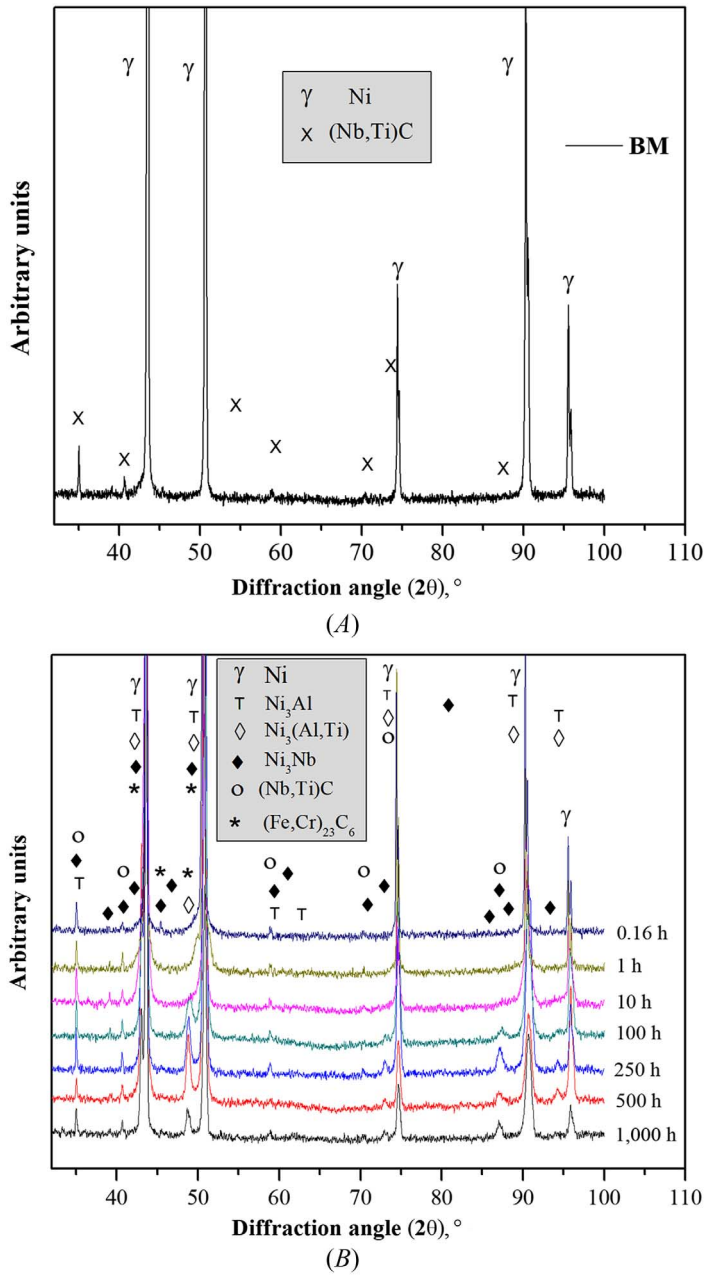


## MICROHARDNESS AND EC

Figure 7 shows the correlation between the induced voltages used for the EC measurements (%IACS conductivity) and HV as a function of the aging time at 750°C.

The annealed condition for the BM provided values of 265 hardness Vickers number (HVN) and 1.38 % IACS. However, it is possible to observe that %IACS and microhardness tend to change as a function of aging time. The hardness increased by approximately 19 % at the initial stage of aging, rising to maximum values at 10 h and corresponding to an increment of ~40 % (fig. 7*A*). Such hardness values correspond to those found by

**FIG. 7**

The behavior of Inconel 718 as a function of aging time: (*A*) microhardness and (*B*) conductivity (%IACS).

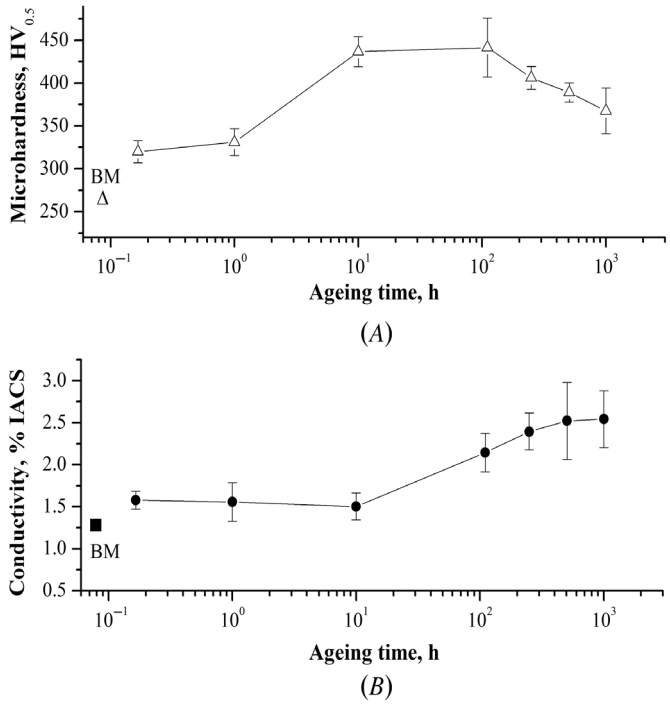


Pereria, although the variations may be due to the difference in the aging temperature.[17] Hardness between 10 and 100 h seems to be constant, but a decrement in hardness is observed for aging times larger than 100 h.

**Figure 7*B*** shows the conductivity evolution. The change in this property due to aging seems to be sufficiently detected using the EC technique. An increment of the %IACS was observed at the initial stage, but no significant changes were detected up to 10 h, where the measurement of the conductivity values decay from 1.57 to 1.50 %IACS. That is to say, before 10 h of aging at 750°C, the transformation of MC carbides to $(Fe,Cr)_{23}C_6$ is not enough to significantly affect the conductivity. This fact might be related to the diffusion process and the formation of vacancies and dislocations. The contribution to the strengthening is mainly caused by the $(Fe,Cr)_{23}C_6$ carbides and the cubic $Ni_3Nb$ γ″ phase after the first 10 h, where the conductivity increases up to 2.14 %IACS, because solid solution elements diffuse to the grain boundaries and the transformation of cubic $Ni_3Nb$ γ″ into the more stable orthorhombic $Ni_3Nb$ δ phase begins. In this context, Abu-Nabah et al.[36] reported that the γ′ and γ″ phases are small precipitates that contribute to the hardening and as a consequence to the electric properties because of the decrement of the solute concentration.

Finally, at an exposition of aging times of 250, 500, and 1,000 h, a reduction of the HV in the Inconel 718 was observed, but the conductivity values increased gradually up to a value of 2.54 %IACS, which can be related to the complete transformation of cubic structure $Ni_3Nb$ γ″ into the orthorhombic $Ni_3Nb$ δ phase, limiting the solid solution elements available. As a first assessment, the findings of this study suggest that values over 2.1 %IACS in this material signal the onset of the Inconel 718 deteriorating due to aging at 750°C.

## Conclusions

From the microstructure observations, the results of EC measurements, and their correlation with the HV of Inconel 718 alloy aged at 750°C for aging periods up to 1,000 h, the following can be concluded:

(a) The aging of Inconel 718 alloy at 750°C induces the precipitation of the γ″ phase for early stages (maximum aging time of 1 h). The hardest conditions were found in the range of 10–100 h of aging.
(b) Through XRD patterns and SEM, the δ phase was identified and correlated well with the increase of %IACS values above 2.14.
(c) The EC technique is sensitive to determining the conductivity in terms of %IACS values when detecting the microstructural evolution of Inconel 718 after isothermal exposition at 750°C. Because of the activation of the diffusion process and the formation of vacancies and dislocations, as well as the subsequent precipitation, growth, and transformation of the intermetallic phases after longer times, the EC technique can detect changes in %IACS after aging for 0.16 h.
(d) According to the EC measurements, the highest HV values were observed in the range of 1.50–2.14 %IACS after exposition at 750°C, which correlate with the evolution of the metastable γ″ phase into the more stable δ phase; higher values of %IACS tend to decrease this property because of the δ phase coarsening.

**DISCLOSURE OF POTENTIAL CONFLICTS OF INTEREST**

We disclose that we are the recipients of financial support for the research, authorship, and publication of this article. This study was supported by PRODEP.

## References

1. J. C. Lippold, S. D. Kiser, and J. N. DuPont, *Welding Metallurgy and Weldability of Nickel-Base Alloys* (Hoboken, NJ: Wiley, 2009).
2. E. Akca and A. Gürsel, "A Review on Superalloys and IN718 Nickel-Based INCONEL Superalloy," *Periodicals of Engineering and Natural Sciences* 3, no. 1 (June 2015): 15–27, http://dx.doi.org/10.21533/pen.v3i1.43
3. C. Slama and M. Abdellaoui, "Structural Characterization of the Aged Inconel 718," *Journal of Alloys and Compounds* 306, nos. 1–2 (June 2000): 277–284, http://dx.doi.org/10.1016/S0925-8388(00)00789-1
4. A. Devaux, L. Nazé, R. Molins, A. Pineau, A. Organista, J. Y. Guédou, J. F. Uginet, and P. Héritier, "Gamma Double Prime Precipitation Kinetic in Alloy 718," *Materials Science and Engineering: A* 486, nos. 1–2 (July 2008): 117–122, http://dx.doi.org/10.1016/j.msea.2007.08.046
5. K. D. Ramkumar, W. S. Abraham, V. Viyash, N. Arivazhagan, and A. M. Rabel, "Investigations on the Microstructure, Tensile Strength and High Temperature Corrosion Behaviour of Inconel 625 and Inconel 718 Dissimilar Joints," *Journal of Manufacturing Processes* 25 (January 2017): 306–322, https://doi.org/10.1016/j.jmapro.2016.12.018
6. S. Ghosh, S. Yadav, and G. Das, "Study of Standard Heat Treatment on Mechanical Properties of Inconel 718 Using Ball Indentation Technique," *Materials Letters* 62, nos. 17–18 (June 2008): 2619–2622, https://doi.org/10.1016/j.matlet.2008.01.001
7. S.-H. Zhang, H.-Y. Zhang, and M. Cheng, "Tensile Deformation and Fracture Characteristics of Delta-Processed Inconel 718 Alloy at Elevated Temperature," *Materials Science and Engineering: A* 528, nos. 19–20 (July 2011): 6253–6258, https://doi.org/10.1016/j.msea.2011.04.074
8. L. C. M. Valle, L. S. Araújo, S. B. Gabriel, J. Dille, and L. H. de Almeida, "The Effect of δ Phase on the Mechanical Properties of an Inconel 718 Superalloy," *Journal of Materials Engineering and Performance* 22, no. 5 (November 2013): 1512–1518, https://doi.org/10.1007/s11665-012-0433-7
9. C. Camerini, C. Temke, W. Kelb, H. Ostermeyer, and D. Stegemann, "Application of Automated Eddy Current Techniques for Off-Shore Inspection," in *Non-destructive Testing '92*, ed. C. Hallai and P. Kulcsar (Oxford, UK: Elsevier, 1992), 254–258, https://doi.org/10.1016/B978-0-444-89791-6.50057-3
10. D. Marino, J.-Y. Kim, A. Ruiz, Y.-S. Joo, J. Qu, and L. J. Jacobs, "Using Nonlinear Ultrasound to Track Microstructural Changes due to Thermal Aging in Modified 9%Cr Ferritic Martensitic Steel," *NDT & E International* 79 (April 2016): 46–52, http://dx.doi.org/10.1016/j.ndteint.2015.12.002
11. A. Ruiz, N. Ortiz, A. Medina, J.-Y. Kim, and L. J. Jacobs, "Application of Ultrasonic Methods for Early Detection of Thermal Damage in 2205 Duplex Stainless Steel," *NDT & E International* 54 (March 2013): 19–26, http://dx.doi.org/10.1016/j.ndteint.2012.11.009
12. N. Ortiz, F. F. Curiel, V. H. López, and A. Ruiz, "Evaluation of the Intergranular Corrosion Susceptibility of UNS S31803 Duplex Stainless Steel with Thermoelectric Power Measurements," *Corrosion Science* 69 (April 2013): 236–244, http://dx.doi.org/10.1016/j.corsci.2012.12.008
13. A. N. Lasseigne, D. L. Olson, H.-J. Kleebe, and T. Boellinghaus, "Microstructural Assessment of Nitrogen-Strengthened Austenitic Stainless-Steel Welds Using Thermoelectric Power," *Metallurgical and Materials Transactions A* 36, no. 11 (November 2005): 3031–3039, https://doi.org/10.1007/s11661-005-0075-6
14. K. V. Rajkumar, B. P. C. Rao, B. Sasi, A. Kumar, T. Jayakumar, B. Raj, and K. K. Ray, "Characterization of Aging Behaviour in M250 Grade Maraging Steel Using Eddy Current Non-destructive Methodology," *Materials Science and Engineering: A* 464, nos. 1–2 (August 2007): 233–240, http://dx.doi.org/10.1016/j.msea.2007.02.006

15. H. Czichos, T. Saito, and L. E. Smith, eds., *Springer Handbook of Metrology and Testing*, 2nd ed. (Berlin: Springer Berlin, Heidelberg, 2011), https://doi.org/10.1007/978-3-642-16641-9
16. R. Chandrasekar, A. M. Frishman, B. F. Larson, C. C. H. Lo, and N. Nakagawa, "Effects of Microstructure on Eddy Current Residual Stress Characterization of Shot-Peened Inconel 718," *JOM* 64, no. 2 (February 2012): 257–264, https://doi.org/10.1007/s11837-012-0234-3
17. D. Pereira, T. Clarke, R. Menezes, and T. Hirsch, "Effect of Microstructure on Electrical Conductivity of Inconel 718 Alloys," *Materials Science and Technology* 31, no. 6 (July 2015): 669–676, https://doi.org/10.1179/1743284714Y.0000000638
18. W. C. Liu, F. R. Xiao, M. Yao, Z. L. Chen, Z. Q. Jiang, and S. G. Wang, "Relationship between the Lattice Constant of ϒ Phase and the Content of δ Phase, γ″ and γ′ Phases in Inconel 718," *Scripta Materialia* 37, no. 1 (July 1997): 59–64, https://doi.org/10.1016/S1359-6462(97)00064-X
19. V. M. A. Silva, C. G. Camerini, J. M. Pardal, J. C. G. de Blás, and G. R. Pereira, "Eddy Current Characterization of Cold-Worked AISI 321 Stainless Steel," *Journal of Materials Research and Technology* 7, no. 3 (July–September 2018): 395–401, https://doi.org/10.1016/j.jmrt.2018.07.002
20. C. Camerini, R. Sacramento, M. C. Areiza, A. Rocha, R. Santos, J. M. Rebello, and G. Pereira, "Eddy Current Techniques for Super Duplex Stainless Steel Characterization," *Journal of Magnetism and Magnetic Materials* 388 (August 2015): 96–100, https://doi.org/10.1016/j.jmmm.2015.04.034
21. S. Azadian, L.-Y. Wei, and R. Warren, "Delta Phase Precipitation in Inconel 718," *Materials Characterization* 53, no. 1 (September 2004): 7–16, https://doi.org/10.1016/j.matchar.2004.07.004
22. G. V. Vander and E. Manilova, "Metallographic Techniques for Superalloys," *Microscopy and Microanalysis* 10, no. S02 (August 2004): 690–691, https://doi.org/10.1017/S1431927604883442
23. M. Durand-Charre, ed., *The Microstructure of Superalloys*, 1st ed. (London: Routledge, 1968), https://doi.org/10.1201/9780203736388
24. A. Agnoli, M. Bernacki, R. E. Logé, J.-M. Franchet, J. Laigo, and N. Bozzolo, "Understanding and Modeling of Grain Boundary Pinning in Inconel 718," in *Superalloys 2012*, ed. E. S. Huron, R. C. Reed, M. C. Hardy, M. J. Mills, R. E. Montero, P. D. Portella, and J. Telesman (Warrendale, PA: The Minerals, Metals & Materials Society, 2012), 73–82, https://doi.org/10.1002/9781118516430.ch8
25. N. Anbarasan, B. K. Gupta, S. Prakash, P. Muthukumar, R. Oyyaravelu, R. J. F. Kumar, and S. Jerome, "Effect of Heat Treatment on the Microstructure and Mechanical Properties of Inconel 718," *Materials Today: Proceedings* 5, no. 2, part 2 (March 2018): 7716–7724, https://doi.org/10.1016/j.matpr.2017.11.448
26. A. J. Ardell, "Precipitation Hardening," *Metallurgical Transactions A* 16, no. 12 (December 1985): 2131–2165, https://doi.org/10.1007/BF02670416
27. J. Lan, H. Huang, H. Mao, and L. Hua, "Phase Transformation and Grain Growth Behaviors of Superalloy IN718 during Heat Treatment," *Materials Today Communications* 24 (September 2020): 101347, https://doi.org/10.1016/j.mtcomm.2020.101347
28. S. Mahajan, C. S. Pande, M. A. Imam, and B. B. Rath, "Formation of Annealing Twins in f.c.c. Crystals," *Acta Materialia* 45, no. 6 (June 1997): 2633–2638, https://doi.org/10.1016/S1359-6454(96)00336-9
29. B. Geddes, H. Leon, and X. Huang, *Superalloys: Alloying and Performance* (Materials Park, OH: ASM International, 2010).
30. L. Liu, K. Tanaka, A. Hirose, and K. Kobayashi, "Effects of Precipitation Phases on the Hydrogen Embrittlement Sensitivity of Inconel 718," *Science and Technology of Advanced Materials* 3, no. 4 (January 2002): 335–344, https://doi.org/10.1016/S1468-6996(02)00039-6
31. C. Slama, C. Servant, and G. Cizeron, "Aging of the Inconel 718 Alloy between 500 and 750 °C," *Journal of Materials Research* 12, no. 9 (September 1997): 2298–2316, https://doi.org/10.1557/JMR.1997.0306
32. L. Wenchang, X. Furen, Y. Mei, C. Zonglin, W. Shaogang, and L. Weihong, "Quantitative Phase Analysis of Inconel 718 by X-ray Diffraction," *Journal of Materials Science Letters* 16, no. 9 (May 1997): 769–771, https://doi.org/10.1023/A:1018553703030
33. S. Gao, J.-S. Hou, Y.-A. Guo, and L.-Z. Zhou, "Phase Precipitation Behavior and Tensile Properties of As-Cast Ni-Based Superalloy during Heat Treatment," *Transactions of Nonferrous Metals Society of China* 28, no. 9 (September 2018): 1735–1744, https://doi.org/10.1016/S1003-6326(18)64817-4
34. X. Z. Qin, J. T. Guo, C. Yuan, C. L. Chen, J. S. Hou, and H. Q. Ye, "Decomposition of Primary MC Carbide and Its Effects on the Fracture Behaviors of a Cast Ni-Base Superalloy," *Materials Science and Engineering: A* 485, nos. 1–2 (June 2008): 74–79, https://doi.org/10.1016/j.msea.2007.07.055
35. M. Fisk, J. Andersson, R. du Rietz, S. Haas, and S. Hall, "Precipitate Evolution in the Early Stages of Ageing in Inconel 718 Investigated Using Small-Angle X-ray Scattering," *Materials Science and Engineering: A* 612 (August 2014): 202–207, http://dx.doi.org/10.1016/j.msea.2014.06.036
36. B. A. Abu-Nabah, W. T. Hassan, D. Ryan, M. P. Blodgett, and P. B. Nagy, "The Effect of Hardness on Eddy Current Residual Stress Profiling in Shot-Peened Nickel Alloys," *Journal of Nondestructive Evaluation* 29, no. 3 (September 2010): 143–153, https://doi.org/10.1007/s10921-010-0072-6